Article

Ultrasensitive Ebola Virus Detection Based on Electroluminescent Nanospheres and Immunomagnetic Separation

Zhen Wu, Jiao Hu, Tao Zeng, Zhi-Ling Zhang, Jian-Jun Chen, Gary Wong, Xiang-Guo Qiu, Wenjun Liu, George F. Gao, Yuhai Bi, and Dai-Wen Pang

Anal. Chem., **Just Accepted Manuscript** • DOI: 10.1021/acs.analchem.6b04632 • Publication Date (Web): 26 Dec 2016

Ultrasensitive Ebola Virus Detection Based on Electroluminescent Nanospheres and Immunomagnetic Separation

Zhen Wu[†], Jiao Hu[†], Tao Zeng[†], Zhi-Ling Zhang[†,*], Jian-Jun Chen[‡,§], Gary Wong[‡,⊥], Xiang-Guo Qiu[¶], Wen-Jun Liu[‡,⊥], George F. Gao[‡,⊥,#], Yu-Hai Bi[‡,⊥,#,*], Dai-Wen Pang[†]

[†]Key Laboratory of Analytical Chemistry for Biology and Medicine (Ministry of Education), College of Chemistry and Molecular Sciences, State Key Laboratory of Virology, Wuhan University, Wuhan, 430072, P. R. China.

[‡]Center for Influenza Research and Early-warning (CASCIRE), Chinese Academy of Sciences, Beijing 100101, China.

[§]CAS Key Laboratory of Special Pathogens and Biosafety, Wuhan Institute of Virology, Chinese Academy of Sciences, Hubei 430071, China.

[¶]Special Pathogens Program, National Microbiology Laboratory, Public Health Agency of Canada; Department of Medical Microbiology, University of Manitoba, Winnipeg, Manitoba R3E 3R2, Canada.

[⊥]CAS Key Laboratory of Pathogenic Microbiology and Immunology, Institute of Microbiology, Chinese Academy of Sciences, Beijing 100101, China.

[#]Shenzhen Key Laboratory of Pathogen and Immunity, State Key Discipline of Infectious Disease, Shenzhen Third People's Hospital, Shenzhen 518112, China.

*Corresponding author: Zhi-Ling Zhang, Email: zlzhang@whu.edu.cn. Yu-Hai Bi, Email: Beeyh@im.ac.cn.

ABSTRACT: The 2014–16 Ebola virus (EBOV) outbreak in West Africa has attracted widespread concern. Rapid and sensitive detection methods are urgently needed for diagnosis and treatment of the disease. Here, we propose a novel method for EBOV detection based on efficient amplification of electroluminescent nanospheres (ENs) coupled with immunomagnetic separation. Uniform ENs are made by embedding abundant amounts of CdSe/ZnS quantum dots (QDs) into copolymer nanospheres through simple ultrasound. Compared to QDs, ENs can enhance electroluminescence (ECL) signals by approximately 85-fold, achieving signal-to-background ratio high enough for EBOV detection. The introduction of magnetic nanobeads (MBs) can selectively separate targets from complex samples, simplifying the operation process and saving time. The presence of MBs can amplify ECL by approximately 3-fold, improving detection sensitivity. By integration of ENs with MBs, a sensitive electroluminescence biosensor is established for EBOV detection. The linear range is 0.02–30 ng/mL with a detection limit of 5.2 pg/mL. This method provides consistent reproducibility, specificity, anti-interference ability, and is highly promising in clinical diagnosis applications.

Introduction

Ebola virus (EBOV), first documented in 1976, is a lethal pathogen, causing severe hemorrhagic fever in humans with a fatality rate up to 90%.[1] The 2014–16 EBOV outbreak in West Africa has attracted widespread attention, with a total of 28,603 laboratory-confirmed cases, including 11,301 deaths reported to the World Health Organization.[2–4] Rapid and sensitive detection methods are crucial for the control and diagnosis of EBOV disease.[5] Traditional methods, including ELISA[6,7] and RT-PCR,[8,9] are commonly used for EBOV detection. However, the sensitivity in ELISA is low and not informative of active infection, limiting its application in real time detection,[10] whereas RT-PCR needs continuous regulation of temperature, precision instruments, professional operation, and is vulnerable to environment interference. Therefore, fast and sensitive methods for EBOV detection are necessary. There are currently many assays based on complementary pairs of oligonucleotide chain or antigen-antibody reaction,[11] the luminescence resonance energy transfer between upconversion nanoparticles and AuNPs,[10] single particle interferometric reflectance imaging,[12] and optofluidic nanoplasmonic[13], which have been used for EBOV detection. However, these methods need complex instruments, are tedious to operate and are generally time-consuming. The development of low-cost, rapid, sensitive and selective alterative detection methods are important.

Electroluminescence (ECL), which is triggered by an electrochemical reaction between electrogenerated species, has advantages of high sensitivity, low-cost, simple optical setup, and low background signal without the need for an external light.[14]

Since the first report on the ECL of silicon nanoparticles in dimethyl formamide (DMF) and acetonitrile by Bard *et al*. in 2002,[15] quantum dots (QDs) ECL based on integration of QDs with ECL has received much attention, such as CdSe, Ag_2Se, CdTe, and PbS.[16–19] Owing to its small size, size-dependent optical properties, and good stability against photobleaching, the integration of QDs with ECL can improve the accuracy and sensitivity of analysis. However, compared to traditional ECL reagents, such as $Ru(bpy)_3^{2+}$ and luminol,[20,21] the ECL efficiency of QDs is relatively low, hindering practical applications. Many amplification strategies based on nanoparticles,[22] enzymes,[23] and cycle amplifying[24] have been proposed to enhance the sensitivity of QDs ECL. In 1977, Bard *et al*.[25] first noted that the application of coreactants can effectively improve ECL intensity. Several coreactants, such as tripropylamine (TPA),[20] H_2O_2,[21] and $K_2S_2O_8$[22] have been widely used. For example, Chen *et al*. recently reported that the dual coreactants of H_2O_2 and $K_2S_2O_8$ can enhance ECL intensity over 100-fold.[26] Compared with annihilation, coreactants can overcome the limited potential window of a solvent or poor anion or cation stability.[26] Moreover, the ECL of QDs tends to surface electron-hole recombination,[27] resulting in broad or shoulder peaks, lowering the spectral selectivity in practical detection. The surface states of QDs can be changed by doping metal ions[27–29] or composition with other nanomaterials.[30–32] Meanwhile, several nanomaterials, such as Au nanoparticles and carbon nanotubes can be modified on the electrode surface to increase the electron transfer rate.[20,33] Currently, QDs ECL has been widely applied in the detection of cells,[21] DNA,[24] and protein.[27] However, novel signal amplification

methods are still needed to improve the practicability and sensitivity of QDs ECL.

To achieve sensitive ECL detection, the existing challenge is to avoid the interference of complex samples. Beneficial characteristics, such as small size, super paramagnetism, water solubility, fast magnetic response, and rich carboxyl or amino functional groups, mean that magnetic nanobeads (MBs) have been broadly applied in the detection of cells, virus, protein and DNA.[34–37] Antibody-modified MBs can rapidly enrich and separate EBOV from complex samples without sample pretreatment, saving detection time and simplifying the operation process. However, transferring the magnetic immunocomplex from solution to the electrode surface is still an important issue. One approach is to add solution onto the electrode surface or immerse the electrode into the solution to form complexes,[38] but this method is time-consuming, unstable, and can easily contaminate the electrode surface. Another approach is to place a magnet under the homemade electrode bottom to fabricate a magnetic electrode.[39] For ECL, the light is collected and amplified by a photomultiplier placed at the bottom, but the magnet at the electrode bottom will hinder the spread of light. Therefore, it is necessary to prepare a type of electrode, which not only quickly captures magnetic compounds, but also allow the spread of light together with high electrochemical activity.

Here, we propose a sensitive method for EBOV detection using prepared electroluminescent nanospheres (ENs), immunomagnetic nanobeads (IMBs), and magnetic gold nanoisland film electrode (M-AuE) as signal markers, capture probes, and working electrode, respectively. ENs greatly enhances the ECL efficiency of QDs

because a single EN can encapsulate hundreds of QDs. In view of its rapid magnetic response, IMBs can separate targets from complex samples without interference. The fabricated M-AuE can quickly capture the magnetic immunocomplex onto the surface to record ECL signals. As shown in Scheme 1, IMBs first capture and separate EBOV from complex samples in a centrifuge tube based on the specific reaction of antigen-antibody. Sandwich composites are then formed on the MBs by adding polyclonal antibody (pAb) modified ENs (IENs) into the solution. Finally, magnetic immunocomplexes are captured onto the M-AuE surface and a strong ECL signal can be obtained by inserting the electrode into a solution of $K_2S_2O_8$.

Experimental Section

Reagents and Instruments. Hydrophobic CdSe/ZnS QDs were purchased from JiaYuan Quantum Dots Co., Ltd (Wuhan). FITC-labeled goat anti-horse IgG (FITC-IgG) was purchased from Alexa 488 (Jackson Immunoresearch Labs Inc.). *N*-hydroxysuccinimide (NHS) was purchased from thermo. Bovine serum albumin (BSA), *N*-(3-Dimethylaminopropyl)-*N′*-ethylcarbodiimide hydrochloride (EDC), and $HAuCl_4$ were purchased from Sigma-Aldrich. Poly(dimethylsiloxane) (PDMS) was purchased from GE (GE Toshiba Silicones. Co., Ltd., Japan). Inactivated EBOV and EBOV GP-specific monoclonal antibody (mAb) and polyclonal antibody (pAb) were obtained from Professor Xiangguo Qiu (Public Health Agency of Canada) or the Center for Influenza Research and Early-warning (CASCIRE), Chinese Academy of Sciences. H7N9 avian influenza virus (H7N9 AIV), H5N1 AIV, Pseudo-rabies virus (PRV), Newcastle disease virus (NDV) were obtained from CASCIRE.

Electrochemical assays were performed on a CHI 660a electrochemical workstation (CH Instruments, Inc.). Electroluminescent detection was acquired on a MPI-EII electroluminescence analyzer workstation (Remex analysis Instrument Co., Ltdl, Xian). Dynamic light scattering (DLS) measurements were performed on a Zetasizer Nano ZS instrument (Malvern). TEM images were obtained by a FEI Tecnai G2 20 TWIN electron microscope. Scanning electron microscopy (SEM) (ZEISS SIGMA FESEM) and atomic force microscope (AFM) (Veeco Instruments Inc.) were used to measure the surface structure of homemade electrodes.

Fabrication of ENs and IENs. Uniform and dispersive poly(styrene/acrylamide) copolymer nanospheres (Pst-AAm-COOH) were prepared according to the method previously reported by our group.[40,41] The ENs were fabricated by embedding many hydrophobic CdSe/ZnS QDs into Pst-AAm-COOH. First, 1.8 mL Pst-AAm-COOH was added into a centrifuge tube followed by centrifuging for 20 min at 18,400 xg. The precipitate was washed with ethanol twice. Meanwhile, moderate QDs were centrifuged for 3 min at 13,800 xg. The supernatant was removed into another centrifuge tube. Triploid volumetric ethanol was added and the mixture was centrifuged at 13,800 xg for 5 min. The precipitation was blown for 10 s by argon and 650 μL swelling agent (5:95 v/v chloroform/butanol) was added. After ultrasonic dispersion, the solution was added into the nanospheres followed by ultrasound for 30 min. Moderate hexane was added and centrifuged for 5 min at 6,900 xg. The precipitate was twice washed with ethanol. Finally, 1 mL ultrapure water was added and ultrasound was applied for 1 h to obtain ENs.

To prepare IENs, 100 μL ENs was centrifuged for 2 min at 11,500 xg. Two hundred microliters of 5 mM EDC/NHS was then added into the precipitate, followed by reaction at 37 ℃ for 30 min. After centrifuging for 2 min at 10,350 xg, the precipitate was washed 3 times with 0.1 M phosphate buffer solution (PBS). Four hundred microliters of PBS containing 10 μL 0.02 mg/mL pAb was then added and reacted at 37 ℃ for 4 h. After centrifuging for 2 min at 10,350 xg and washing with PBS 3 times, IENs were blocked with 100 μL 1% BSA and stored at 4 ℃ for further use.

Preparation of M-AuE. First, ITO glasses were cut into 3 × 1 cm rectangles and soaked in piranha solution (7:3 v/v concentrated H_2SO_4/30% H_2O_2; *Caution! The piranha solution should be handled with extreme care*) for 2 min. After washing with ultrapure water, slides were paced into a 3-aminopropyltriethoxysilane (APTES) solution (40 μL APTES, 186 μL methanol, 2 μL acetate, and 980 μL ultrapure water) overnight. The slides were then removed to a small dish containing 4.3 mL ultrapure water, 600 μL 1% $HAuCl_4$, and 100 μL $NH_3 \cdot H_2O$, followed by reacting for 5 min at 25 ℃ with gentle shaking (120 rpm). Subsequently, the slides were soaked into 5 mL ice water containing 0.19 mg $NaBH_4$ for 10 min, followed by incubating in 5 mL ultrapure water containing 154 μL $HAuCl_4$ and 0.26 mg hydroxylamine hydrochloride ($NH_2OH \cdot HCl$) for 20 min to obtain gold nanoisland film modified slides.

Meanwhile, 5 g PDMS (10:1 w/w RTV615A/RTV615B) was added onto silicon wafer and put on the spin coater with 600 rpm for 15 s to obtain 200 μm thin membranes. After heating at 75 ℃ for 30 min, the PDMS was peeled off, cut into 2 × 1 cm rectangles and punched with a 3 mm diameter needle. The PDMS cell was

irreversibly bonded to the above slides to fabricate 3 mm AuE. Finally, a 4 mm diameter and 1 mm thick circular magnet was fixed at the back of AuE by PDMS to prepare M-AuE.

Sensitive EBOV Detection. Based on the layer-by-layer (LBL) assembly method reported by our group previously,[37,42] superparamagnetic MBs were prepared to capture the target from complex systems. First, antibody modified MBs (IMBs) were fabricated by mixing 10 μL 10 mg/mL MBs with 200 μL pH 6.1 0.1 M PBS containing 0.1 M EDC/NHS. After reacting at 37 °C for 30 min and washing with pH 7.2 PBS 3 times, 200 μL pH 7.2 PBS containing 0.05 mg/mL mAb was added and incubated overnight to obtain IMBs. The IMBs were blocked with 200 μL 1% BSA and stored at 4 ℃ for further use.

The EBOV detection was based on a sandwich immunoreaction. First, 20 μL IMBs were mixed with different concentrations of EBOV in 200 μL pH 7.2 PBS and reacted at 37 ℃ with gentle shaking for 30 min. The virus-IMBs were then separated with a magnetic scaffold to remove the suspension and washed 3 times with PBS. Subsequently, 200 μL pH 7.2 PBS containing 10 μL IENs was added into virus-MBs and incubated at 37 ℃ for 20 min to obtain IENs-virus-IMBs compounds. Finally, a M-AuE was used to capture the compounds and inserted into a beaker containing 5 mL detection solution (0.1 M pH 7.2 PBS consisted of 0.1 M KCl and 0.1 M $K_2S_2O_8$) with an Ag/AgCl as reference and a Pt wire as counter electrode. Then the cyclic voltammetry (CV) from −1.65 to 0 V with a 200 mV/s scanning rate and a 900 V voltage of photomultiplier tube (PMT) was performed to record ECL signals.

Results and Discussion

Characterization of ENs and MBs.

Based on the embedding method, an abundance of QDs were embedded into Pst-AAm-COOH by simple ultrasound, as illustrated in Figure 1A. Transmission electron microscope (TEM) images of Pst-AAm-COOH and CdSe/ZnS QDs were shown in Figure S1A-B in the Supporting Information. The fluorescence microscopic image of ENs indicated the excellent optical stability of QDs (Figure S1C, Supporting Information). The TEM image (Figure 1B) displayed well-dispersed ENs and many nanoparticles distributed around in the ENs (Figure 1B insert), showing the successful preparation of ENs. By randomly counting the size of 300 ENs, the average diameter was calculated to be approximately 268 ± 8 nm with a variation coefficient of 4.2% (Figure 1C), indicating the uniformity of ENs. Furthermore, the hydrated size of nanospheres increased from 252.5 to 273.4 nm (Figure S2A, Supporting Information), according with the TEM results. Accordingly, the surface charge (ζ potential) changed from −42.9 to −38.9 mV (Figure S2B, Supporting Information), which verified that ENs could keep good dispersibility and rich carboxyl functional groups on the surface. As shown in Figure S3A in the Supporting Information, the ECL spectrum of ENs demonstrated a single peak at 610 nm, close to that of the fluorescence emission peak (PL) of 604 nm, indicating the well-passivated surface of CdSe/ZnS QDs.[30,43]

Compared to QDs, ENs could amplify ECL signals by approximately 85-fold under the same concentration of 10 pM (Figure 1D). The possible reasons may be: (1) High ECL efficiency of core-shell CdSe/ZnS QDs resulted from the well-passivated surface;

(2) a single nanosphere can encapsulate hundreds of QDs to provide large signal amplification.[44] It has been calculated that 332 ± 8 QDs can be embedded into one nanosphere;[41] (3) QDs in the nanospheres still kept good optical and electrochemical properties. To investigate the effect of antibody modification on the ECL of ENs, the ECL intensities of ENs and IENs were recorded (Figure S3B, Supporting Information). The comparability demonstrated the negligible influence of antibody modification on the ECL intensity of ENs. Therefore, the use of ENs as a biomarker in electroluminescent biosensor could obtain strong ECL signals, improving the sensitivity of the method.

In order to capture and separate EBOV from complex samples, MBs were generated based on a LBL method. Owing to the coordination effect between the amino of polyethyleneimine (PEI) and metal elements on the surface of nanoparticles, five layers Fe_3O_4 nanoparticles were assembled on the surface of Pst-AAm-COOH.[42] The TEM image (Figure 2A) showed that the MBs were uniform in size and well-dispersed in water with a diameter of about 380 nm. As shown in Figure 2B, antibody modified MBs (IMBs) could selectively capture EBOV from samples due to the specific antigen-antibody reaction and the immunomagnetic separation ability of MBs. The amount of mAb per MB was estimated to be about 200 and details were shown in Figure S4 in the Supporting Information, demonstrating the rich binding sites as well as the availability of IMBs in efficient capture of EBOV. From the magnetic hysteresis loop (Figure 2C), the high saturation magnetization of MBs (35.4 emu/g) without retentivity could be observed, indicating the magnetic property of

MBs. Moreover, almost 100% MBs could be captured by a magnetic scaffold in 60 s (Figure 2D), demonstrating a rapid magnetic response. According to the dynamic light scattering (DLS) of MBs (Figure 2E-F), the hydrated size and ζ potential were about 391.5 nm and −29.5 mV, respectively, indicating good solubility and abundant surface functional groups for further modification.

In summary, these results show that we have prepared a novel ENs capable of efficient ECL amplification and MBs, which could selectively capture and separate target virus from complex samples.

Preparation and Characterization of M-AuE.

To capture the magnetic immunocomplex onto the surface of working electrodes and ensure the transparent of the electrolytic cell bottom for light collection, a new kind of M-AuE was generated. Based on the seeding and growing method, a layer of gold nanoisland film was generated on the surface of ITO glasses,[45,46] as illustrated in Figure 3A. Scanning electron microscopy (SEM) was used to characterize the surface morphology of glasses. As shown in Figure 3B, many sphere, ellipsoid, and saddle nanoisland-shaped nanostructures were distributed on the glass surface, demonstrating the successful modification of golden nanoisland film. Atomic force microscopy (AFM) was further used to characterize the surface roughness (Figure 3C). The bare ITO glass was flat with a surface roughness (Rq) of 2.66 nm. After modification, the surface became uneven and the Rq increased to 12.5 nm, indicating successful preparation. To prepare uniform golden nanoisland film, the seeding concentration of $HAuCl_4$ was optimized and the corresponding SEM images were shown in Figure S5

in the Supporting Information. Individual Au nanoparticles appeared at low concentrations, growing into nanoisland film at higher concentrations, and forming a continuous gold film at very high concentrations.[46]

To prepare the electrode of a fixed size, a 200 μm thin PDMS membrane with a 3 mm hole was covered onto the surface of AuE to construct a 3 mm electrode, due to the excellent impermeability and stability of PDMS. The magnetic AuE (M-AuE) was fabricated by placing a 4 mm diameter and 1 mm thick circular magnet on the back of the AuE. Compared to ITO electrodes, M-AuE obtained obvious redox peak by the CV from −0.2 to 1.1 V in 0.5 M H_2SO_4 (Figure S6A, Supporting Information), indicating the successful preparation of M-AuE as well as its good electrochemical activity. According to the charge of reduction peaks, the surface area of M-AuE was calculated to be approximately 3.05 mm^2. The CVs of ten M-AuEs in 0.5 M H_2SO_4 indicated that M-AuEs were uniform enough to implement high-throughput parallel tests required for EBOV detection (Figure S6B, Supporting Information). As shown in Figure 3C, the ECL intensity of M-AuE was 2.3 times stronger than the ITO electrode under the same concentration of ENs, improving the sensitivity of the detection. The reason may be that Au nanoislands modification not only increased the specific surface area, but also accelerated the electron transfer rate between electrode and ENs.[20,47] The ITO electrode surface became dark when the potential reached −1.2 V, indicating the reduction of ITO and its unavailability in cathodic electroluminescent detection. However, the fabricated M-AuE remained stable even when the potential was lowered to −2 V, effectively solving the reduction problem of ITO.

These results showed that the prepared M-AuE can solve the instability of ITO under relatively negative potentials, effectively capture magnetic immunocomplex on the electrode surface, and enhance ECL signals.

Feasibility of the Immunosensor for EBOV Detection.

Based on the integration of M-AuE with efficient ECL amplification of ENs together with fast magnetic separation ability of MBs, a sensitive electroluminescent immunosensor was constructed for EBOV detection. From −1.65 to 0 V, the CVs and ECL curves were recorded under different conditions to examine the feasibility and selectivity of the method. As shown in Figure 4A, AuE or ENs/AuE appeared as a strong reduction peak at −1.17 V and some bubbles without $K_2S_2O_8$ (a, b), which may have resulted from the H^+ reduction. With $K_2S_2O_8$, another reduction peak at −0.75 V could be seen on the bare AuE surface, which may be the reduction of $K_2S_2O_8$ (c). Furthermore, the peak of ENs/AuE at −0.75 V became unclear and the peak at −1.17 V changed to −1.19 V, coupled with an increasing current (d), demonstrating ENs reduction. Correspondingly, only when ENs and $K_2S_2O_8$ existed at the same time, a strong ECL signal could be obtained (Figure 4B), ignoring the interference of background. The ECL mechanism of QDs can be shown as follows: when the potential scanned negatively, CdSe/ZnS QDs were reduced to negatively charged species $(CdSe/ZnS)^{-\bullet}$. Meanwhile, $S_2O_8^{2-}$ at the electrode surface was reduced to the strong oxidant $SO_4^{-\bullet}$. $(CdSe/ZnS)^{-\bullet}$ then reacted with $SO_4^{-\bullet}$ and produced an excited state species $(CdSe/ZnS)^*$, which emitted light accompanying by returning to the ground state.[43] The equations corresponding to each step of the emission reactions are

as follows:

$$\mathrm{CdSe/ZnS} + \mathrm{e^-} \rightarrow \mathrm{(CdSe/ZnS)^{-\bullet}} \quad (1)$$

$$\mathrm{S_2O_8^{2-}} + \mathrm{e^-} \rightarrow \mathrm{SO_4^{-\bullet}} + \mathrm{SO_4^{2-}} \quad (2)$$

$$\mathrm{SO_4^{-\bullet}} + \mathrm{(CdSe/ZnS)^{-\bullet}} \rightarrow \mathrm{(CdSe/ZnS)^*} + \mathrm{SO_4^{2-}} \quad (3)$$

$$\mathrm{(CdSe/ZnS)^*} \rightarrow \mathrm{CdSe/ZnS} + h\nu \quad (4)$$

In order to investigate the feasibility in EBOV detection, the curves of ECL-time and ECL-potential under different reaction conditions were recorded, as shown in Figure 4C-D. There was nearly no ECL signal in the absence of ENs, indicating the background signal of $K_2S_2O_8$ was negligible (a). Without mAb (b), pAb (c), or virus (d), the ECL signals were almost zero resulting from the unsuccessful sandwich immunoreaction on the surface of MBs. However, a strong ECL signal appeared in the presence of 10 ng/mL EBOV (e), demonstrating good specificity for the EBOV detection method.

The experiment conditions were further optimized to improve the signal-to-background ratio. The coreactant concentration of $K_2S_2O_8$ greatly influenced the ECL intensity of ENs, as shown in Figure 5A. ECL signals increased with $K_2S_2O_8$ concentrations and tended to a platform at 0.1 M. For cathodic electroluminescence, the negative potential also affected ECL signals. The highest signal-to-background ratio achieved when the potential was low to −1.65 V (Figure 5B). Two, rather than one, ECL peaks appeared with a potential that is more negative than −1.65 V, which may have resulted from the electron injection to a higher energy as well as new electron-hole recombination.[19,32] Moreover, ECL signals increased with the scanning

rate and 200 mV/s resulted in a maximum signal-to-background ratio (Figure 5C). ECL signals became unstable with further increase of the scanning rate, which was unsuitable for analysis. Finally, the pH of the buffer was discussed and pH 7.2 PBS lead to the largest ECL signal (Figure 5D). Therefore, the highest signal-to-background ratio of 35 could be obtained at the conditions of 0.1 M $K_2S_2O_8$, −1.65 V potential, 200 mV/s scanning rate, and pH 7.2 PBS, which could be used for sensitive EBOV detection.

Sensitive EBOV Detection.

By using the ENs, MBs, and M-AuE as signal markers, capture probes, and working electrodes, respectively, a novel electroluminescent immunosensor for EBOV detection was generated. Under optimal conditions, the amplification effect of immunomagnetic separation was first examined, as shown in Figure 6A. The application of MBs could amplify ECL signals by approximately 3-fold compared with the absence of MBs. Possible reasons may be the large specific surface area, good magnetic response and fast reaction kinetics of MBs.[34] As shown in Figure 6B, the ECL signals of ENs still displayed excellent stability after continuous 10 scanning circles at the potential range from −1.65 to 0 V, which was suitable for EBOV detection. A small decline appeared afterwards because of the diffusion and reduction of the electroactive substances from the electrode surface, having no effect on detection. The ECL signals increased with EBOV concentrations (Figure 6C) and a good linear range from 0.02 to 30 ng/mL with a detection limit of 5.2 pg/mL at a signal-to-noise ratio of 3 (Figure 6D), which was between 1–5 orders of magnitude

more sensitive than other EBOV detection methods.[6,48,49] The proposed strategy was comparable to recently reported EBOV detection including fluorescence resonance energy transfer between upconversion materials and Au nanoparticles[10] or single particle interferometric reflectance imaging sensor.[12] Possible explanations may be as follows: (1) MBs could rapidly and specifically separate targets from complex samples; (2) compared to QDs, ENs could amplify ECL by approximately 85-fold, providing an efficient ECL amplification strategy; (3) by taking advantage of the good electrochemical activity and magnetic enrichment ability of M-AuE, EBOV could be detected with high sensitivity.

The reliability and reproducibility of a method is necessary for its practical application. The same batch and different batches of MBs were used to test three different concentrations (0.02, 5, and 30 ng/mL) of EBOV samples. As shown in Table 1, the intra-assay coefficient variation (CV) and inter-assay CV were 4.4% and 5.3%, respectively, due to the uniformity, dispersity, and stability of the MBs, indicating good accuracy. Correspondingly, the same and different batches of ENs were also used to perform three parallel experiments. The intra-assay CV and inter-assay CV were calculated to be 3.8% and 4.5%, respectively, demonstrating good reliability. Moreover, in order to examine the storage stability of ENs and IENs, the ECL intensities were continuously recorded for seven weeks, as shown in Figure S7 in the Supporting Information. The stable ECL signals resulted from the good optical stability and biological activity of ENs, further ensuring the repeatability of the method in practical application.

In practical applications, specificity is necessary to avoid the false positive interference and to confirm the early diagnosis of disease. Other viruses, such as H5N1 AIV (8 μg/mL), H7N9 AIV (15 μg/mL), NDV (2 μg/mL), and PRV (10 μg/mL) were used as negative control samples. As shown in Figure 7A, a 20 ng/mL EBOV sample achieved strong ECL signals and control samples were negligible. The ECL of EBOV sample was approximately 18-fold stronger than negative samples, even when their concentrations were 2–3 orders of magnitude more concentrated than EBOV, indicating high selectivity, as well as potential application in complex systems.

EBOV generally exists in complex biological samples, which requires that this detection method has great anti-interference ability. Based on the specific reaction of antigen-antibody and magnetic separation, IMBs could capture and separate targets from samples followed by enriching onto the M-AuE surface to obtain ECL signals. EBOV (20 ng/mL) was added to grinded chicken liver, chicken heart, and chicken serum to prepare EBOV positive samples. Correspondingly, control samples were prepared with the same method without adding EBOV. As shown in Figure 7B, all positive EBOV samples had stronger ECL signals than control samples, demonstrating anti-interference ability and specificity.

In summary, the proposed method for EBOV detection based on ENs and MBs has the advantages of high sensitivity, selectivity, stability, reproducibility, and anti-interference ability.

Conclusions

In summary, a novel electroluminescence biosensor based on the integration of ENs, MBs with M-AuE has been demonstrated for ultrasensitive EBOV detection. Compared to QDs, ENs can amplify ECL intensities by approximately 85-fold, offering an efficient signal amplification strategy. The use of ENs as signal markers can greatly improve the sensitivity of the method. MBs, being used as capture probes, can simplify the operation process and decrease detection time. To capture immunoreaction complex onto the electrode surface and record ECL signals, a homemade M-AuE is prepared, which not only improves the surface area but also solves the redox problem of ITO electrodes under a negative potential. The sensitivity, specificity, and reliability are greatly improved, enabling the method to be applied for EBOV detection with a wide linear range of 0.02–30 ng/mL. As low as 5.2 pg/mL EBOV can be detected in about 2 h without complicated sample pretreatment or sophisticated instruments, showing broad potential in exploring signal amplification electroluminescent biosensors as well as the early diagnosis of EBOV disease.

FIGURES

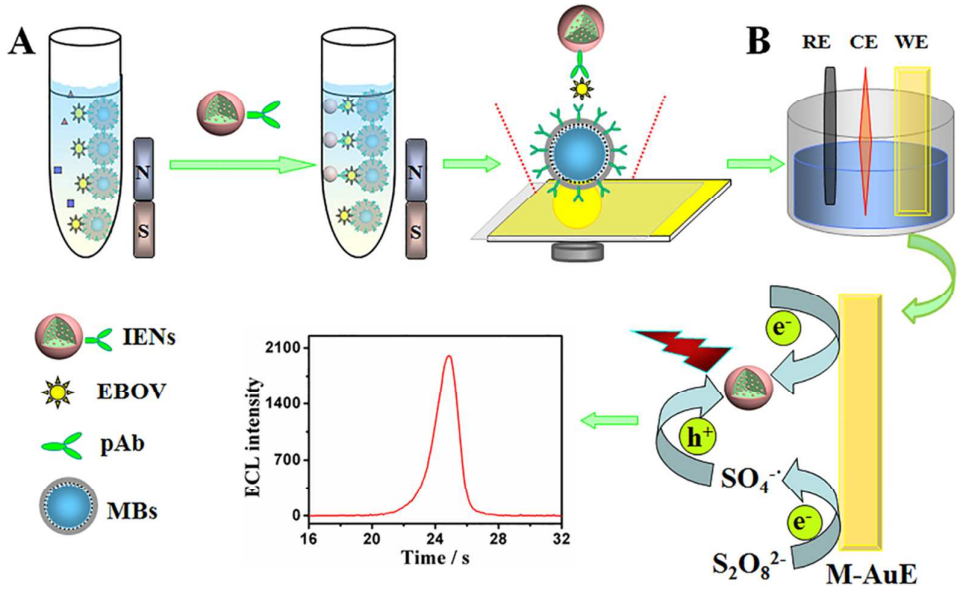

Scheme 1. Illustration of the protocol for electroluminescent detection of EBOV. (A) Sandwich immunoreaction. (B) Electroluminescent detection in $K_2S_2O_8$ solution.

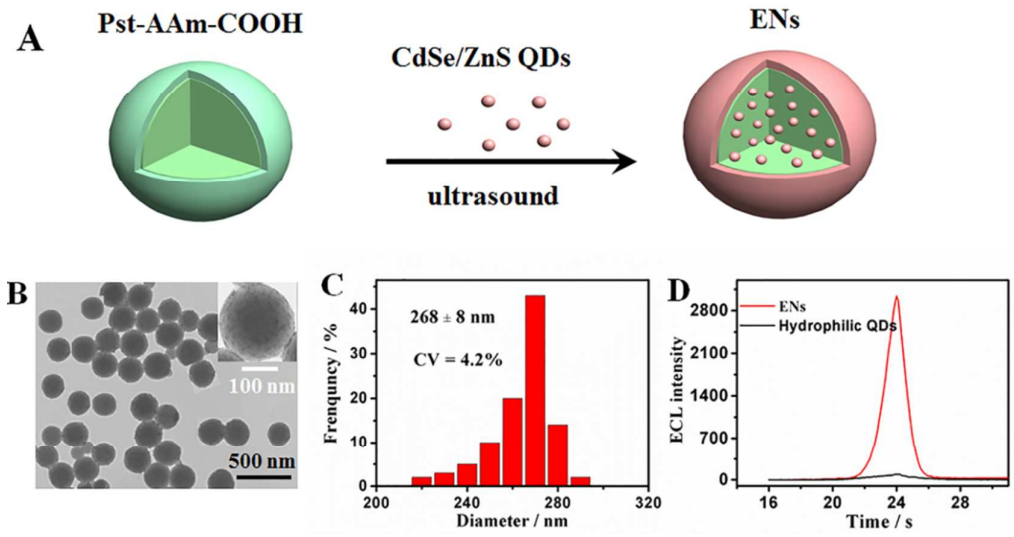

Figure 1. Fabrication and characterization of ENs. (A) Fabrication diagram of ENs. (B) TEM image of the ENs embedded with hydrophobic QDs. Inset: an amplification image of a single EN. (C) Histogram for the size distribution of ENs (n=300). (D) ECL intensity of ENs and hydrophilic QDs at a concentration of 10 pM.

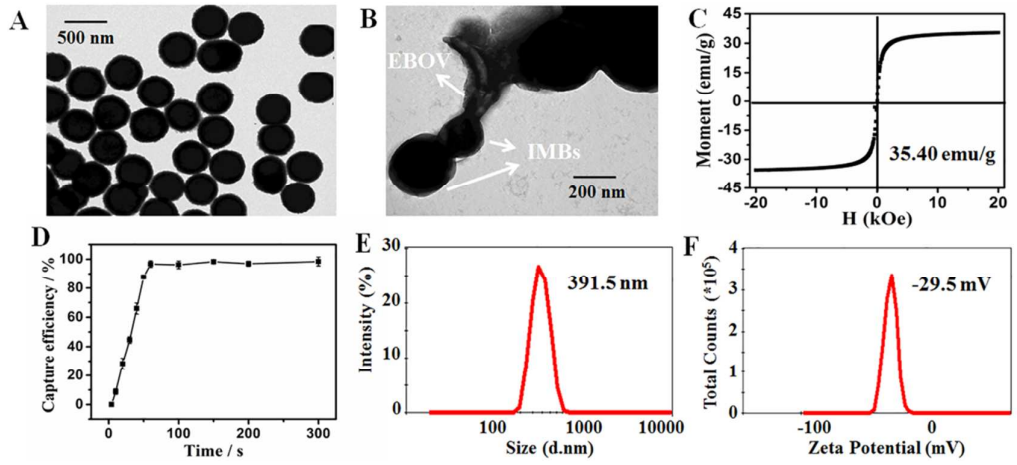

Figure 2. Characterization of MBs. (A) TEM image of MBs. (B) TEM image of IMBs-virus composite. (C) Hysteresis loop of MBs. (D) Capture efficiencies of MBs at different attraction times with a commercial magnetic scaffold. (E) Hydrated particle size of MBs. (F) Surface potential of MBs.

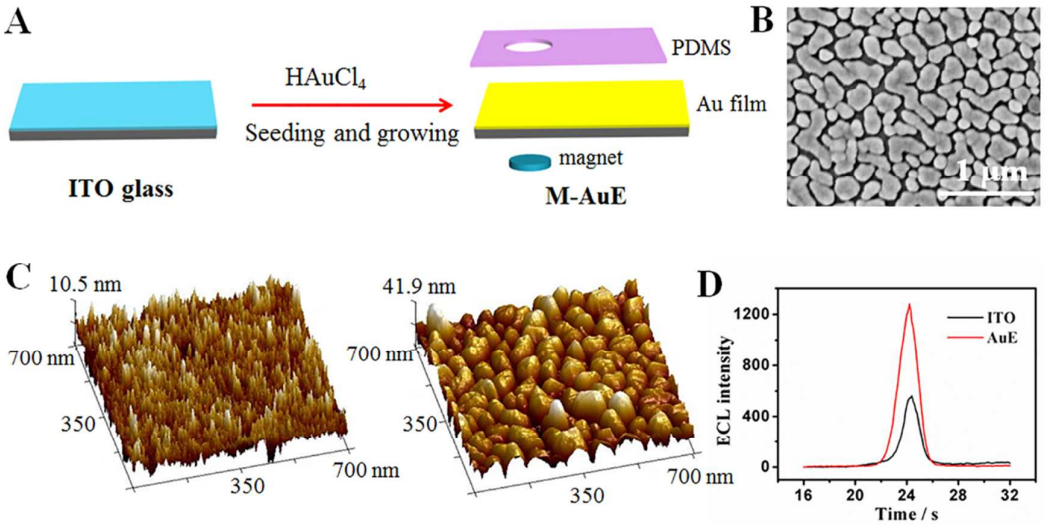

Figure 3. (A) Fabrication diagram of gold nanoisland film electrode (M-AuE). (B) SEM image of AuE surface. (C) AFM images of ITO and AuE surface respectively. (D) ECL intensities of ITO electrode and M-AuE under the same ENs concentration.

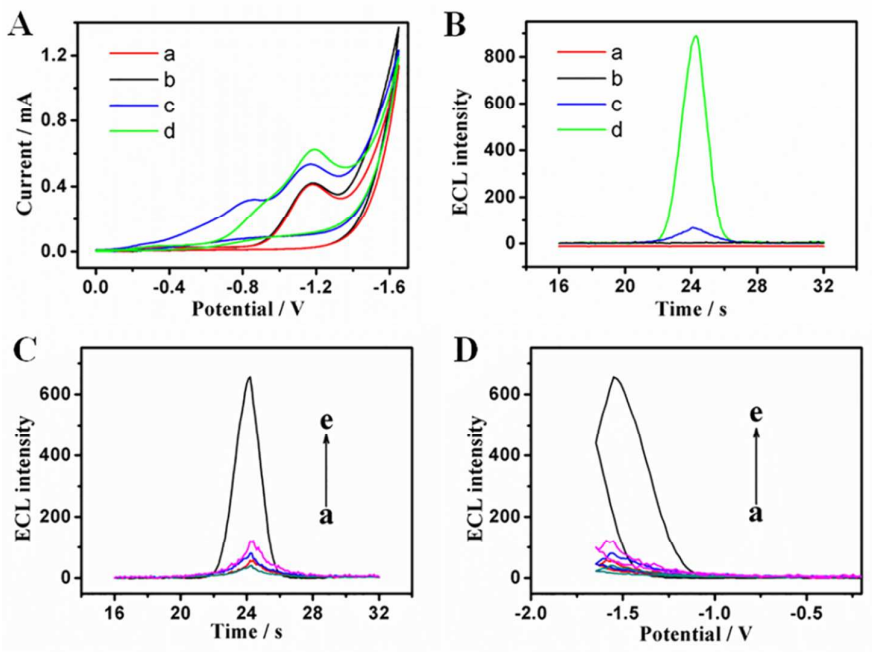

Figure 4. (A) CV and (B) ECL behaviors of (a) bare AuE, (b) ENs/AuE in 0.1 M PBS, and (c) bare AuE, (d) ENs/AuE in 0.1 M PBS containing 0.1 M $K_2S_2O_8$. (C) ECL signals of different modification conditions (a) without ENs, (b) without mAb, (c) without pAb, (d) without virus, (e) 10 ng/mL EBOV. (D) Corresponding ECL-potential curves of (a)-(e).

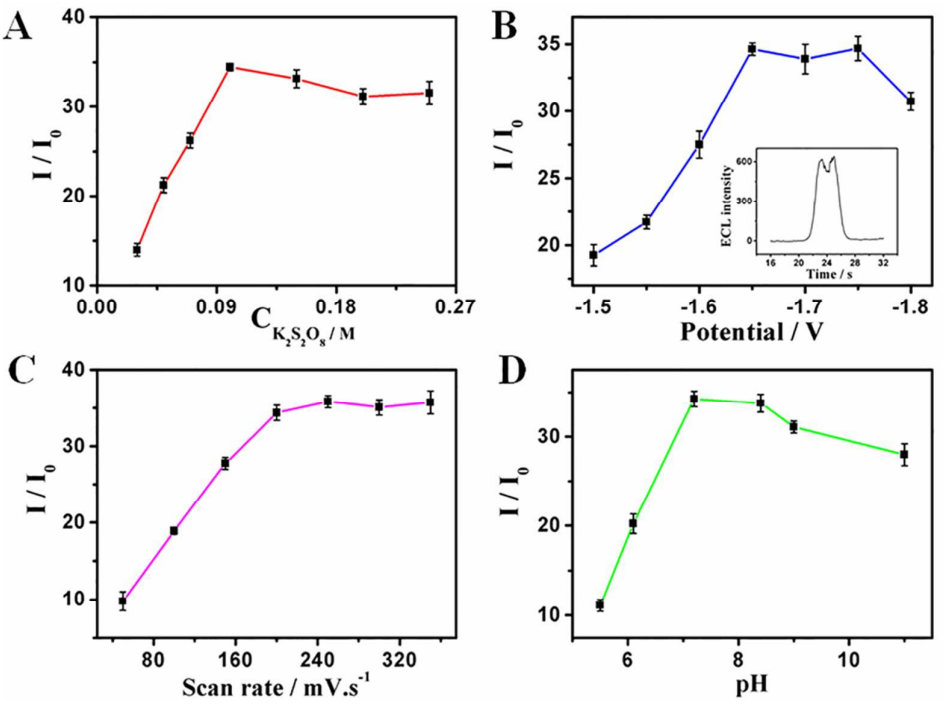

Figure 5. The effects of (A) $K_2S_2O_8$ concentration, (B) negative potential (Inset: Typical ECL signal), (C) scan rate, and (D) pH on the signal-to-background ratio (I: ECL intensity; I_0: Background intensity).

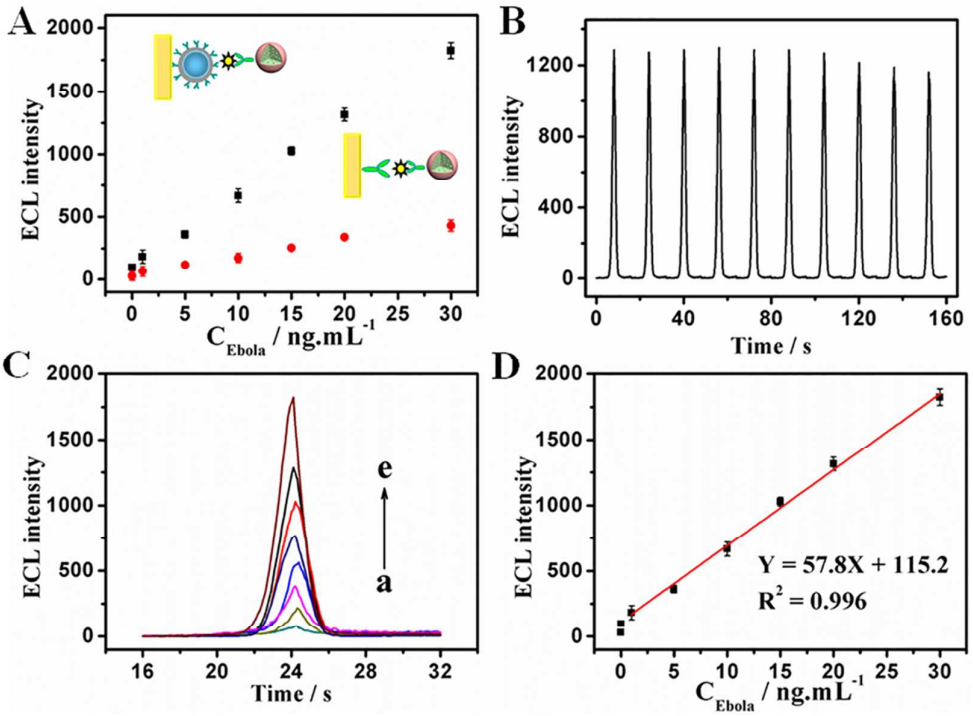

Figure 6. (A) Calibration plots of ECL intensities versus EBOV concentrations by using the same sandwich immunoreaction with MBs (squares) and without MBs (circles). (B) ECL signals after continuous 10 circles at the potential range from −1.65 to 0 V. (C) Typical ECL signals in the presence of different EBOV concentrations. (D) Corresponding linear curve between ECL intensities and EBOV concentrations (0, 0.02, 1, 5, 10, 15, 20, 30 ng/mL).

Table 1 Reproducibility of the ENs-based electroluminescence for EBOV detection

Ebola concentration	Intra-assay			Inter-assay		
(ng/mL)	Mean [a]	SD [b]	CV (%) [c]	Mean [a]	SD [b]	CV (%) [c]
0.02	97	4.5	4.6	106	6.6	6.2
5	361	18.1	5.0	378	21.5	5.7
30	1822	63.0	3.5	1759	70.3	4.0
	Intra-assay variability 4.4%			Inter-assay variability 5.3%		

[a] Values represent the average of the ECL intensity of parallel samples (n=3); [b] values represent the standard deviation of parallel results (n=3); [c] CV=SD/Mean.

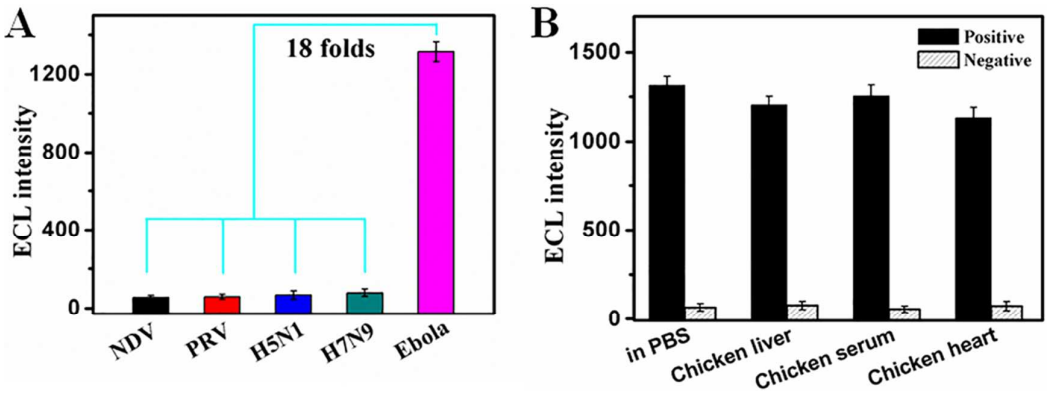

Figure 7. (A) Histogram for the specificity of this method for EBOV detection. (B) ECL intensities of the immunosensor in the presence (black histograms) and absence (white histograms) of EBOV in different complex media.

AUTHOR INFORMATION

Corresponding Author

*Zhi-Ling Zhang, Email: zlzhang@whu.edu.cn; Phone: 0086-27-68756759, Fax: 0086-27-68754067. Yu-Hai Bi, Email: Beeyl@im.ac.cn.

Notes

The authors declare no competing financial interest.

ACKNOWLEDGMENTS

This work was supported by the 863 Program (2013AA032204), the National Science and Technology Major Project (2016ZX10004222), the National Natural Science Foundation of China (21475099, 21535005), and the Natural Science Foundation of Hubei (2014CFA003). Y.B. is supported by the Youth Innovation Promotion Association of Chinese Academy of Sciences (CAS). G.W. is the recipient of a Banting Postdoctoral Fellowship from the Canadian Institutes of Health Research (CIHR) and the President's International Fellowship Initiative from the CAS.

SUPPORTING INFORMATION AVAILABLE

Sections S. 1−S. 7, and Figures S1−S7. Figure S1, characterization of ENs. Figure S2, DLS characterization of ENs. Figure S3, PL and ECL spectrum of ENs. Figure S4, characterization of MBs. Figure S5, preparation and characterization of M-AuE. Figure S6, CVs of ITO electrode and M-AuE. Figure S7, storage stability of ENs and IENs.

REFERENCES

(1) Mohan, G. S.; Li, W.; Ye, L.; Compans, R. W.; Yang, C. *PLoS Pathog.* **2012**, *8*, e1003065.

(2) WHO Website. Ebola virus disease. Accessed 26th October **2016**. http://www.who.int/mediacentre/factsheets/fs103/en/

(3) Tong, Y. G.; Shi, W. F.; Liu, D.; Qian, J.; Liang, L.; Bo, X. C.; Liu, J.; Ren, H. G.; Fan, H.; Ni, M.; Sun, Y.; Jin, Y.; Teng, Y.; Li, Z.; Kargbo, D.; Dafae, F.; Kanu, A.; Chen, C. C.; Lan, Z. H.; Jiang, H.; Luo, Y.; Lu, H. J.; Zhang, X. G.; Yang, F.; Hu, Y.; Cao, Y. X.; Deng, Y. Q.; Su, H. X.; Sun, Y.; Liu, W. S.; Wang, Z.; Wang, C. Y.; Bu, Z. Y.; Guo, Z. D.; Zhang, L. B.; Nie, W. M.; Bai, C. Q.; Sun, C. H.; An, X. P.; Xu, P. S.; Zhang, X. L.; Huang, Y.; Mi, Z. Q.; Yu, D.; Yao, H. W.; Feng, Y.; Xia, Z. P.; Zheng, X. X.; Yang, S. T.; Lu, B.; Jiang, J. F.; Kargbo, B.; He, F. C.; Gao, G. F.; Cao, W. C. *Nature* **2015**, *524*, 93–96.

(4) Ni, M.; Chen, C.; Qian, J.; Xiao, H. X.; Shi, W. F.; Luo, Y.; Wang, H. Y.; Li, Z.; Wu, J.; Xu, P. S.; Chen, S. H.; Wong, G.; Bi, Y.; Xia, Z. P.; Li, W.; Lu, H. J.; Ma, J.; Tong, Y. G.; Zeng, H.; Wang, S. Q.; Gao, G. F.; Bo, X. C.; Liu. D. *Nat. Microbiol.* **2016**, *1*, 16151.

(5) Su, S.; Wong, G.; Qiu, X.; Kobinger, G.; Bi, Y.; Zhou, J. *Lancet. Infect. Dis*. **2016**, *16*, 294–295.

(6) Niikura, M.; Ikegami, T.; Saijo, M.; Kurane, I.; Miranda, M. E.; Morikawa, S. *J. Clin. Microbiol.* **2001**, *39*, 3267–3271.

(7) Krähling, V.; Becker, D.; Rohde, C.; Eickmann, M.; Eroğlu, Y.; Herwig, A.; Kerber, R.; Kowalski, K.; Vergara-Alert, J.; Becker, S. *Med. Microbiol. Immunol.* **2016**, *205*, 173–183.

(8) Sanchez, A.; Ksiazek, T. G.; Rollin, P. E.; Miranda, M. E. G.; Trappier, S. G.; Khan, A. S.; Peters, C. J.; Nichol, S. T. *J. Infect. Dis.* **1999**, *179*, S164–S169.

(9) Ahrberg, C. D.; Manz, A.; Neužil, P. *Anal. Chem.* **2016**, *88*, 4803–4807.

(10) Tsang, M. K.; Ye, W. W.; Wang, G.; Li, J.; Yang, M.; Hao, J. *ACS Nano* **2016**, *10*, 598–605.

(11) Kaushik, A.; Tiwari, S.; Jayant, R. D.; Marty, A.; Nair, M. *Biosens. Bioelectron.* **2016**, *75*, 254–272.

(12) Daaboul, G. G.; Lopez, C. A.; Chinnala, J.; Goldberg, B. B.; Connor, J. H.; Unlü, M. S. *ACS Nano* **2014**, *8*, 6047–6055.

(13) Yanik, A. A.; Huang, M.; Kamohara, O.; Artar, A.; Geisbert, T. W.; Connor, J. H.; Altug, H.

Nano Lett. **2010**, *10*, 4962–4969.

(14) Miao, W. *Chem. Rev.* **2008**, *108*, 2506–2553.

(15) Ding, Z.; Quinn, B. M.; Haram, S. K.; Pell, L. E.; Korgel, B. A.; Bard, A. J. *Science* **2002**, *296*, 1293–1297.

(16) Cui, R.; Gu, Y. P.; Bao, L.; Zhao, J. Y.; Qi, B. P.; Zhang, Z. L.; Xie, Z. X.; Pang, D. W. *Anal. Chem.* **2012**, *84*, 8932–8935.

(17) Hesari, M.; Swanick, K. N.; Lu, J. S.; Whyte, R.; Wang, S.; Ding, Z. *J. Am. Chem. Soc.* **2015**, *137*, 11266–11269.

(18) Zou, G.; Liang, G.; Zhang, X. *Chem. Commun.* **2011**, *47*, 10115–10117.

(19) Wu, P.; Hou, X.; Xu, J. J.; Chen, H. Y. *Chem. Rev.* **2014**, *114*, 11027–11059.

(20) Dong, Y. P.; Chen, G.; Zhou, Y.; Zhu, J. J. *Anal. Chem.* **2016**, *88*, 1922–1929.

(21) Zhang, H. R.; Wang, Y. Z.; Zhao, W.; Xu, J. J.; Chen, H. Y. *Anal. Chem.* **2016**, *88*, 2884–2890.

(22) Jie, G. F.; Liu, P.; Zhang, S. S. *Chem. Commun.* **2010**, *46*, 1323–1325.

(23) Wang, B.; Wang, H.; Zhong, X.; Chai, Y.; Chen, S.; Yuan, R. *Chem. Commun.* **2016**, *52*, 5049–5052.

(24) Yang, L.; Tao, Y.; Yue, G.; Li, R,; Qiu, B.; Guo, L.; Lin, Z.; Yang, H. H. *Anal. Chem.* **2016**, *88*, 5097–5103.

(25) Chang, M. M.; Saji, T.; Bard, A. J. *J. Am. Chem. Soc.* **1977**, *99*, 5399–5403.

(26) Dai, P. P.; Yu, T.; Shi, H. W.; Xu, J. J.; Chen, H. Y. *Anal. Chem.* **2015**, *87*, 12372–12379.

(27) Ma, H.; Li, X.; Yan, T.; Li, Y.; Liu, H.; Zhang, Y.; Wu, D.; Du, B.; Wei, Q. *ACS Appl. Mater. Interfaces* **2016**, *8*, 10121–10127.

(28) Deng, L.; Shan, Y.; Xu, J. J.; Chen, H. Y. *Nanoscale* **2012**, *4*, 831–836.

(29) Tian, C. Y.; Xu, J. J.; Chen, H. Y. *Chem. Commun.* **2012**, *48*, 8234–8236.

(30) Myung, N.; Bae, Y.; Bard, A. J. *Nano Lett.* **2003**, *3*, 1053–1055.

(31) Liu, D.; Wang, L.; Ma, S.; Jiang, Z.; Yang, B.; Han, X.; Liu, S. *Nanoscale* **2015**, *7*, 3627–3633.

(32) Liu, S.; Zhang, Q.; Zhang, L.; Gu, L.; Zou, G.; Bao, J.; Dai, Z. *J. Am. Chem. Soc.* **2016**, *138*, 1154–1157.

(33) Qiu, Z.; Yu, J.; Yan, P.; Wang, Z.; Wan, Q.; Yang, N. *ACS Appl. Mater. Interfaces* **2016**, *8*, 28291–28298.

(34) Wu, Z.; Zhou, C. H.; Chen, J. J.; Xiong, C.; Chen, Z.; Pang, D. W.; Zhang, Z. L. *Biosens. Bioelectron.* **2015**, *68*, 586–592.

(35) Mani, V.; Chikkaveeraiah, B. V.; Patel, V.; Gutkind, J. S.; Rusling, J. F. *ACS Nano* **2009**, *3*, 585–594.

(36) Zhou, C. H.; Zhao, J. Y.; Pang, D. W.; Zhang, Z. L. *Anal. Chem*. **2014**, *86*, 2752–2759.

(37) Wen, C. Y.; Wu, L. L.; Zhang, Z. L.; Liu, Y. L.; Wei, S. Z.; Hu, J.; Tang, M.; Sun, E. Z.; Gong, Y. P.; Yu, J.; Pang, D. W. *ACS Nano* **2014**, *8*, 941–949.

(38) Li, J.; Xu, Q.; Wei, X.; Hao, Z. *J. Agric. Food Chem.* **2013**, *61*, 1435–1440.

(39) Zhou, C. H.; Wu, Z.; Chen, J. J.; Xiong, C.; Chen, Z.; Pang, D. W.; Zhang, Z. L. *Chem. Asian J.* **2015**, *10*, 1387–1393.

(40) Song, E. Q.; Hu, J.; Wen, C. Y.; Tian, Z. Q.; Yu, X.; Zhang, Z. L.; Shi, Y. B.; Pang, D. W. *ACS Nano* **2011**, *5*, 761–770.

(41) Hu, J.; Zhang, Z. L.; Wen, C. Y.; Tang, M.; Wu, L. L.; Liu, C.; Zhu, L.; Pang, D. W. *Anal. Chem.* **2016**, *88*, 6577–6584.

(42) Xie, M.; Hu, J.; Wen, C. Y.; Zhang, Z. L.; Xie, H. Y.; Pang, D. W. *Nanotechnology* **2012**, *23*, 035602.

(43) Liu, S.; Zhang, X.; Yu, Y.; Zou, G. *Anal. Chem.* **2014**, *86*, 2784–2788.

(44) Sardesai, N.; Pan, S.; Rusling, J. *Chem. Commun.* **2009**, *7*, 4968–4970.

(45) Hong, G.; Tabakman, S. M.; Welsher, K.; Wang, H.; Wang, X.; Dai, H. *J. Am. Chem. Soc.* **2010**, *132*, 15920–15923.

(46) Tabakman, S. M.; Chen, Z.; Casalongue, H. S.; Wang, H.; Dai, H. *Small* **2011**, *7*, 499–505.

(47) Wu, Z.; Zhou, C. H.; Pan, L. J.; Zeng, T.; Zhu, L.; Pang, D. W.; Zhang, Z. L. *Anal. Chem.* **2016**, *88*, 9166–9172.

(48) Trombley, A. R.; Wachter, L.; Garrison, J.; Buckley-Beason, V. A.; Jahrling, J.; Hensley, L. E.; Schoepp, R. J.; Norwood, D. A.; Goba, A.; Fair, J. N.; Kulesh, D. A. *Am. J. Trop. Med. Hyg*. **2010**, *82*, 954–960.

(49) Li, Y.; Cu, Y. T. H.; Luo, D. *Nat. Biotechnol.* **2005**, *23*, 885–889.

For TOC only